For submission to JGR

Winter 2015

The Surface Distribution of $\Delta^{14}C$

J. R. Toggweiler
Geophysical Fluid Dynamics Laboratory, NOAA
Princeton, NJ USA

Ellen R. M. Druffel
Department of Earth System Science, University of California, Irvine
Irvine, CA USA

Robert M. Key
Atmospheric and Oceanic Sciences Program, Princeton University
Princeton, NJ USA

Eric D. Galbraith
Earth and Planetary Sciences, McGill University
Montreal, Quebec, CANADA

J. R. Toggweiler is with the Geophysical Fluid Dynamics Laboratory, National Oceanic and Atmospheric Administration, P.O. Box 308, Princeton, NJ, 08542, USA (robbie.toggweiler@noaa.gov)

Ellen R. M. Druffel is with the Department of Earth System Science, University of California, Irvine, Irvine, CA 92687-3100, USA (edruffel@uci.edu)

Robert M. Key is with the Atmospheric and Oceanic Sciences Program, Princeton University, Princeton, NJ 08544 USA (key@princeton.edu)

Eric Galbraith is with the Department of Earth and Planetary Sciences, McGill University, Montreal, Quebec, CANADA H3A 2A7 (eric.galbraith@mcgill.ca)

Abstract

The main upwelling zone for the ocean's deep water is the area south of the Antarctic Circumpolar Current (ACC). The most unambiguous indicator of the upwelling is the low $\Delta^{14}C$ of the surface waters south of the ACC. Here, $\Delta^{14}C$ is mapped across the ocean basins to assess the upwelling north of the ACC. Information is compiled for up to 110 locations during 1940-1954, 1990-1994, and 2003-2006. Our maps show that deep water is drawn up to the surface in the wind-driven upwelling zones around the margins of the basins. It appears to reach the surface two ways. Deep water that is upwelled initially south of the ACC is brought to the surface a second time in the eastern boundary upwelling zones off northern and southern Africa in the Atlantic, off Costa Rica and Peru in the Pacific, and off Sumatra in the Indian Ocean. Deep water also reaches the surface directly off Oman and Kamchatka in the northwest corners of the Indian and Pacific, respectively. The upwelling around the ocean's margins is not generally thought to be part of the ocean's overturning circulation. The results here show that it is. We argue at the end of the paper that the eastern boundary upwelling, in particular, is no less important to the ocean's overturning and heat transport than the upwelling along the ACC.

Introduction

The deep waters of the ocean are famously deficient in ^{14}C because of their isolation from the atmosphere. The deficits vary from place to place in a way that reflects the ocean's overturning circulation. Here we consider a less exploited part of the ^{14}C distribution − the ^{14}C deficits at the ocean's surface. The goal of this paper is to map the surface deficits in order to see what they reveal about the upwelling portion of the overturning circulation. We are aided in this task by the fact that ^{14}C deficits can persist at the surface for ten years or more owing to the slow gas exchange process for ^{14}C (Broecker and Peng, 1974).

^{14}C deficits are reported as $\Delta^{14}C$, the per mil departure of the measured $^{14}C/^{12}C$ ratio in a sample from a standard reference ratio after a correction for isotopic fractionation (Stuiver and Polach, 1977). The reference ratio is the atmospheric $^{14}C/^{12}C$ ratio during the late 19th century. In this context, the deep ocean is depleted in ^{14}C by about 17% and average deep water has a $\Delta^{14}C$ of −170‰ (Stuiver et al., 1983).

Most of the ocean's deep water is now thought to be brought up to the surface south of the ACC (Marshall and Speer, 2012). Indeed, the ^{14}C deficits around Antarctica are very large and not unlike the deficits in the deep ocean (Toggweiler and Samuels, 1993). Our interest here is in the deficits north of the ACC. The upwelling north of the ACC is thought to be hard to observe because it is associated with weak upward motions that are spread across the ocean basins (Drijfhout et al., 2013). Our maps show that this assertion is not really true: the upwelling north of the ACC is actually easy to observe and is readily characterized.

Toggweiler, Dixon, and Broecker (1991), hereon TDB91, give us an idea of what to expect. They used eight "pre-bomb" $\Delta^{14}C$ measurements from the tropical Pacific to examine the upwelling in a vintage circulation model from the 1980s. The overturning in the model delivered abyssal water slowly up into the thermocline. The abyssal water was then funneled up to the surface via the equatorial divergence. So, the simulated distribution featured a $\Delta^{14}C$ minimum along the equator. But the eight measurements indicated that the lowest $\Delta^{14}C$ values would be found in the upwelling zone off Peru instead. TDB91 then traced the water off Peru back to the area where Subantarctic Mode Water

(SAMW) is formed along the northern edge of the ACC. This showed two things: first, the widespread upwelling in the model was seen to be largely fictitious; second, low-$\Delta^{14}C$ water was seen to reach the surface in the tropical Pacific *after* it is brought up to the surface initially in the Southern Ocean.

Here, we query a much larger data set that includes the Atlantic and Indian Oceans. The first order of business is to see if SAMW or Antarctic Intermediate Water (AAIW) from the ACC reaches the surface in Peru-like environments elsewhere. A second is to see if water from the deep ocean reaches the surface directly in places other than the Southern Ocean. A new data-model comparison is then carried out to show how the upwelling in these areas is represented in a modern ocean circulation model.

2. Anthropogenic Perturbations

Relatively few observations were available to TDB91 because of the nuclear weapons tests that took place during the 1950s and early 1960s. The bomb tests, as they are called, added a spike of new ^{14}C atoms to the atmosphere that altered the steady-state distribution that had prevailed before the bomb tests. Bomb ^{14}C is first detected in the ocean in a coral growth band from the year 1955 (Fallon and Guilderson, 2008). The bomb tests also occurred in the midst of a long-term decline in the surface $\Delta^{14}C$ due to the burning of fossil fuels (the Suess Effect). The latter was a minor effect before 1950 but has become a much larger effect in recent decades.

Figure 1 shows the fossil fuel and bomb perturbations in three corals that grew in the North Atlantic between 1900 and 2010. During the early 1900s the average $\Delta^{14}C$ at the three locations was about −45‰. By 1950 the $\Delta^{14}C$ in the three corals had declined to −55‰ due to the burning of fossil fuels. By 1970 the surface $\Delta^{14}C$ had risen to +140‰ in response to the bomb tests. A maximum value of +160‰ is recorded in the late 1970s. The first ocean-wide survey of $\Delta^{14}C$ took place during the 1970s when surface $\Delta^{14}C$ values were at their highest levels (Broecker et al., 1985).

A more detailed survey was carried out during the 1990s as part of the World Ocean Circulation Experiment (WOCE). **Figure 2** provides an unfiltered view of the surface $\Delta^{14}C$ across the Pacific at this time. The highest values (red shades) were found

along 30°N and 30°S. The lowest values (blue shades) were found along the southern edge of the map at 60°S. As anticipated by TDB91, the lowest values in the equatorial zone (green shades) are south of the equator and close to Peru.

While bomb ^{14}C was clearly still present during WOCE, an aspect of the pre-bomb pattern had begun to re-emerge. Among TDB91's eight pre-bomb values, the highest value (−42‰ from Okinawa; Konishi et al., 1982) and the lowest value (−72‰ from the Galapagos Islands; Druffel, 1981) differed by 30‰. This difference was a response to the circulation, especially the upwelling in the eastern equatorial Pacific. The 30‰ difference then increased to 150‰ during the 1970s due to the enhanced buildup of bomb ^{14}C in the area near Okinawa (see Figure 7 in TDB91). By the 1990s, however, the difference between these locations had fallen back to about 50‰. So, while bomb ^{14}C was still present, it was more dispersed or "smoothed out."

Pre-bomb observations have become available from some three dozen new locations since the publication of TDB91. The new observations, along with the smoothing out of the bomb effect above, led us to think that the pattern of circulation-induced $\Delta^{14}C$ differences might be reconstructed and mapped across all three ocean basins.

3. $\Delta^{14}C$ Anomaly Maps

The measurement errors for $\Delta^{14}C$ are not small in relation to the differences noted above. The error for an individual sample varies from 2‰ up to 8‰ depending on the way the measurements were made. Seawater observations also tend to be fairly noisy because they are subject to weather-related water mass changes (McDuffee and Druffel, 2007) and to seasonal mixing with subsurface waters (Druffel et al., 2010). The surface $\Delta^{14}C$ values during WOCE were also changing over time, as seen in **Figure 1**.

To improve the signal-to-noise ratio for our maps, we identified 110 "regions of interest" where multiple $\Delta^{14}C$ measurements are available during one of three time windows. Our regions are skewed toward areas where corals and shells were collected during pre-bomb time. They also tend to be skewed toward areas that are likely to be influenced by upwelling, e.g. areas with the green, yellow, and blue shades in **Figure 2**. All the measurements from a given region and within a given time period are averaged

and the regional averages are normalized by subtracting the contemporary $\Delta^{14}C$ averages from Bermuda or Okinawa. The resulting $\Delta^{14}C$ differences, called "anomalies," are used to illustrate the circulation influence on the surface $\Delta^{14}C$. To avoid confusion, anomalies are given without units; $\Delta^{14}C$ measurements will always be given with the ‰ symbol.

Bermuda and Okinawa are remote from any upwelling areas and tend to have the highest $\Delta^{14}C$ values in their respective oceans. As such, the surface waters near Bermuda and Okinawa are influenced more by the changing atmospheric $\Delta^{14}C$. The surface waters elsewhere are influenced by both the atmospheric $\Delta^{14}C$ and the circulation, so the differences, our anomalies, should mainly reflect the circulation. The same normalization is applied in Section 7 to the $\Delta^{14}C$ distributions generated by our ocean circulation model.

Our Atlantic regions of interest are listed in **Table S1** in the Supplemental Material. Their locations are given on the map in **Figure S1**. Our Pacific and Indian regions are listed in **Tables S3** and **S5**, respectively, and their locations are given in **Figures S3 and S5**. All the $\Delta^{14}C$ measurements used to construct our regional averages are listed along with their sources in **Tables S2, S4, and S6**. The time windows with the most information are 1940-1954, the early 1990s, and the mid 2000s. The data from the 1990s are mainly from seawater samples collected during WOCE. The data from the 2000s are mainly from seawater samples collected by the Climate Variability and Predictability Program (CLIVAR) of the World Climate Research Program.

For reference, the actual WOCE measurements from the Atlantic are shown in **Figure S2** in the Supplemental Material. The WOCE measurements from the Pacific are shown in **Figure S4**. (This is the same map shown in **Figure 2**.) The WOCE measurements from the Indian Ocean are shown in **Figure S6** and later here as **Figure 5**.

4. Anomaly Maps for the Atlantic Ocean

4a. Atlantic - Pre-Bomb Period (1940-1954)

Our maps for the pre-bomb period are based entirely on measurements from corals and shells. Two maps have been constructed for the Atlantic. The first is for the decade of the 1940s (**Figure 3a**). The second is for 1950-54 (**Figure 3b**). The anomalies for Bermuda are zero, by definition, and are shown within the black squares. The $\Delta^{14}C$

averages for Bermuda, i.e. the reference values that are subtracted from the averages of the other regions, are −47 and −48‰, respectively (**Table S2**).

The other anomalies on the maps are shown within green squares. The anomalies in the green squares are all negative. This simply means that the ^{14}C deficits at these locations are larger than the contemporary deficit at Bermuda. In the text to follow, a more negative anomaly is considered a larger anomaly. Differences of 3 units or less are generally not significant.

The preparation of two pre-bomb maps is motivated by the coral record from the south coast of Puerto Rico in Kilbourne et al. (2007) − one of the three Atlantic records in **Figure 1**. Kilbourne et al. found that the $\Delta^{14}C$ off Puerto Rico fell by about 7‰ between the 1940s and the early 1950s. Citing Schmitz and Richardson (1991), Kilbourne et al. attributed the change to a stronger Atlantic Meridional Overturning Circulation (AMOC) that carried more low-$\Delta^{14}C$ water from the South Atlantic into the Caribbean Sea.

We wanted to see if the $\Delta^{14}C$ change at Puerto Rico could be corroborated by similar changes elsewhere. The anomaly at Puerto Rico was −8 during the 1940s and increased to −14 during 1950-54. **Figures 3a and 3b** show that the anomaly off Belize increased from −7 to −12 while the anomaly off Florida increased from −9 to −11. The change off Florida is not significant. Meanwhile, anomalies in the Gulf of Mexico and off the northern coast of South America changed by 1 to 3 units in the opposite direction. So, we do not see a $\Delta^{14}C$ change that is coherent across the region.

The largest anomaly on either map is the −30 value off northwest Africa in **Figure 3a**. This value comes from four shells collected off Mauritania and Senegal during the 1940s (**Table S2**). The area off northwest Africa is a well known coastal upwelling area (Mittelstaedt, 1983). **Figure 3a** also includes an anomaly of −21 from a shell collected near the southern tip of Africa (Dewar et al., 2012). This location is within the Benguela upwelling zone but is several hundred kilometers south of the core area off Namibia (Nelson and Hutchings, 1983; Gordon et al., 1995).

Another prominent feature in both maps is the east-west contrast across the northern North Atlantic. The anomalies off Norway and southern Great Britain on the eastern side of the basin are quite small, −6 and −8 in **Figure 3a** and −7 in **3b**. In con-

trast, the anomalies from Georges Bank, the Grand Banks, and the Labrador Sea on the western side clump together around −23. The small anomalies in the east seem to reflect the northward flow of the AMOC, much of which is near the surface and in continuous contact with the atmosphere.

The larger anomalies in the west are explained by the cyclonic circulations in the areas north of the Gulf Stream and in the Labrador Sea. Tanaka et al. (1990) measured low $\Delta^{14}C$ values in eight shells collected from Georges Bank between 1866 and 1937. They attributed the low values to the upwelling of AAIW in this area. The deficits in the Labrador Sea could also be from the Arctic Ocean. Eiríksson et al. (2011) show that the East Greenland Current intermittently delivers low-$\Delta^{14}C$ Arctic water to the shelf north of Iceland.

4b. Atlantic - WOCE Era (1990-1998)

The WOCE sampling program was limited north of Iceland and in the South Atlantic. Fortunately, several complementary sampling efforts are available to fill these holes. The data base in **Table S2** includes 36 samples collected by Nydal (1998) mainly in the eastern, tropical, and South Atlantic, eight samples collected near the mouth of the Amazon River by Druffel et al. (2005), and six samples from the South Atlantic Ventilation Experiment (SAVE) that were collected in 1989. The data base also includes information from corals and shells that were collected off Norway, Iceland, Bermuda, Florida, and Puerto Rico.

Two maps have been constructed for the WOCE Era. The first map (**Figure 3c**) is for the main interval of WOCE sampling from 1990 to 1994. It includes the six SAVE samples from 1989. The second map (**Figure 3d**) is for 1997-98 when a series of late WOCE cruises took place. The Bermuda reference values for the two periods are 113 and 94‰, respectively (**Table S2**).

The map in **Figure 3c** includes three positive anomalies, +16 along 25°N in the middle of the North Atlantic and two values of +4 along 30°S in the South Atlantic. The negative anomalies on this map are also larger than those on the pre-bomb maps. Basically, areas like Bermuda continued to have more bomb ^{14}Cduring the 1990s and the

extra ^{14}C elevates our Bermuda reference. Subtracting a higher reference value leads to larger negative anomalies elsewhere. A different situation is encountered in the subpolar zone where the −6 and −7 anomalies off Norway during pre-bomb time give way to an anomaly of −53 during WOCE. The −14 and −16 anomalies north and south of Iceland in **Figure 3a** increase to −78. These large subpolar anomalies reflect mixing with deeper water that remained relatively uncontaminated with bomb ^{14}C.

The map in **Figure 3c** provides a more detailed look at the tropical Atlantic. It features anomalies of −37 and −35 near the upwelling zone off northwest Africa and anomalies of −22 and −17 off Puerto Rica and Florida, respectively. The −37 anomaly off northwest Africa is derived from seven seawater samples, four of which were collected within 100 km of the coast. The other three were collected about 1200 km from the coast. The four near-shore samples would have an anomaly of −42 (see listing for Region 20 in **Table S2**). The map also has an anomaly of −41 off southern Africa. This value comes from three seawater samples collected about 250 km offshore from the border area between South Africa and Namibia (Region 29 in **Table S2**).

The WOCE map also includes information from four locations within the equatorial zone. These anomalies fall between −22 and −26. As such, they are smaller than the anomalies off Africa and are larger than the anomalies from Puerto Rico and Florida. Moreover, the −26 anomaly from the equator in **Figure 3c** is only 1-3 units larger than the anomalies to the north and south. This is not a significant difference. The same tendency is seen in our CLIVAR map below (**Figure 3e**). This shows that the equatorial divergence is not a source of low-$\Delta^{14}C$ water.

This information has important consequences for our understanding of the AMOC. Basically, the AMOC enters the Atlantic as a subsurface flow of cool and relatively fresh water off southern Africa (Gordon et al., 1992; Sloyan and Rintoul, 2001). It then exits from the tropics off the coast of Florida. According to Schmitz and Richardson (1991), about 60% of the northward flow of the AMOC off Florida is at the surface. So, somewhere between 35°S and 25°N, more than half of the northward flow of the AMOC is brought up to the surface.

The largest ^{14}C deficits in the tropical Atlantic are found near the upwelling zones off the coast of Africa. There are no deficits of this size anywhere else. We take this to mean that the upwelling zones off Namibia and northwest Africa are the places where the AMOC is routed up to the surface. The idea that these upwelling zones are part of the AMOC has not been considered before. The deficits off Africa seem to extend across the Atlantic to Florida. We take this as an indication of how far the deficits from Africa are able to spread. The spreading reflects both the volume of the upwelling and the slow decline of the initial deficits via the gas exchange process for ^{14}C.

Our WOCE map for 1997-98 in **Figure 3d** includes a repeat of the east-west section taken along 25°N during 1992. The anomalies along the section are uniformly smaller in 1998. This is because the $\Delta^{14}C$ values at Bermuda and in the middle of the 25°N section declined more than the values at the other locations. The most striking new results on the map for 1997-98 are the −33 and −37 anomalies along the north coast of South America. These anomalies are much larger than any anomalies seen in this area before or since but they are not unlike the anomalies seen off northern and southern Africa between 1990 and 1994.

4c. Atlantic - CLIVAR Era (2003-2005)

Our CLIVAR map in **Figure 3e** is based on samples collected between 2003 and 2005. The Bermuda reference value is 81‰ (**Table S2**).

The range of anomalies during 2003-2005 is considerably smaller than the range in the early 1990s. This is largely a response to the ongoing burning of fossil fuels. Sometime after the year 2000 the $\Delta^{14}C$ of the atmosphere fell below the highest $\Delta^{14}C$ values in the ocean (as shown in Figure 5 in Druffel et al., 2010). So, areas like Bermuda actually began losing ^{14}C to the atmosphere while the upwelling areas continued to gain ^{14}C. This changeover flattens the $\Delta^{14}C$ distribution and reduces the anomalies on our maps. With the exception of the two locations north of South America, the anomalies in the tropical Atlantic range from −11 to −17. Five samples collected within 250 km of the equator (Region 24, **Table S2**) have an anomaly of −12, which is indistinguishable from the values to the north and south.

Our CLIVAR map includes evidence for a large temporal change north of Iceland. During the 1940s the surface waters north and south of Iceland had more-or-less the same $\Delta^{14}C$ values. During WOCE both areas had anomalies of −78. During CLIVAR, the anomaly south of Iceland decreased to −21 while the anomaly north of Iceland remained at −75. The temporal change would seem to be due to a change in circulation north of Iceland. The shelf north of Iceland is subject to extensive changes in water properties as older fresher polar water from the East Greenland Current and younger, saltier Atlantic water from the Irminger Current take turns dominating the North Icelandic shelf over time (Knudsen et al., 2004; Massé et al., 2008; Eiríksson et al., 2011; and Jónsson and Valdimarsson, 2012). It would appear that the anomaly from 2005 records an invasion of older polar water onto the shelf.

5. Anomaly Maps for the Pacific Ocean

5a. Pacific - Pre-Bomb Period (1940-1954)

A single pre-bomb map has been constructed for the Pacific in **Figure 4a**. The time window is 1940-1954. The Okinawa reference value is –40‰ (**Table S4**). As before, the anomaly for Okinawa is zero and is shown within the black square.

The largest pre-bomb anomalies, –53, –61, and –47, are from Kodiak Is., Vancouver Is., and southern California, respectively. The location closest to the upwelling zone off Peru is the Galapagos Islands, which has an anomaly of –28. The most well resolved feature of the map in **Figure 4a** is the band of anomalies between –15 and –22 that stretches across the Pacific in the equatorial zone. The band extends all the way to Palau, –15, and Makassar Strait, –16. As in **Figure 2**, the largest equatorial anomalies are south of the equator and west of Peru.

TDB91 determined that the water upwelling off Peru was originally SAMW. They also determined that the SAMW in the South Pacific had a pre-bomb $\Delta^{14}C$ of –75 to –80‰. The South Pacific water destined to upwell off Peru would therefore have had an anomaly of –35 to –40 relative to Okinawa. So the water that actually reached the surface off Peru presumably had an anomaly that was larger than –28 (Galapagos) and smaller than –35 (SAMW). This is essentially the same deficit seen off northwest Africa

during pre-bomb time. The deficits off Kodiak Is., Vancouver Is., and southern California were notably larger. The water upwelling in these areas must therefore have a deeper source, presumably a source in the deep North Pacific. The source of the water upwelling in these areas is considered more fully in Section 8a of the Discussion.

5b. Pacific - WOCE Era (1991-1993)

The anomaly map for the Pacific in **Figure 4b** is based on samples collected between 1991 and early 1994. The Okinawa reference value is 115‰. It is based on six coral measurements and sixteen seawater samples collected between 21° and 35°N along WOCE leg P10 (Region 10 in **Table S4**). Two regions east of Okinawa along 30°N have anomalies of 0 and +1. The Easter Island area has an anomaly of +9. The Easter Island anomaly is based on five seawater samples collected near the intersection of WOCE lines P18 and P6 about 3° south of Easter Island (Region 38 in **Table S4**).

As expected from **Figure 2**, the anomaly off Peru, –59, is larger than the anomaly from the Galapagos Islands, –48. The anomalies to the west of Peru are also more negative than the anomalies to the north or south. Our WOCE map has three anomalies for the equator itself, –21, –22, and –41. All three fall between lower values to the south and higher values to the north. So, as in the Atlantic, the ^{14}C deficits along the equator are unremarkable.

The map in **Figure 4b** has some very large anomalies in the subpolar region in the north. The area near the Kamchatka Peninsula, in particular, has an anomaly of −134. This is the largest anomaly on any of our maps. The Gulf of Alaska has an anomaly of −95. These areas are located within the western and eastern centers of the subpolar gyre, respectively, where the Ekman divergence draws subsurface water up to the surface. Again, the anomaly off Southern California, −88, is significantly larger than the anomaly off Peru, −59.

5c. Pacific - CLIVAR Era (2003-2006)

The CLIVAR map for the Pacific in **Figure 4c** is relatively sparse but it documents a large temporal change between 1950 and the mid 2000s. During pre-bomb time, Okinawa had the highest $\Delta^{14}C$ in the ocean. This distinction passes to Easter Island

during WOCE. This area continued to have the highest $\Delta^{14}C$ during CLIVAR with an anomaly of +4. Along these lines, the anomalies at Hawaii and Easter Island were quite similar during pre-bomb time, −11 and −7, but diverged dramatically during WOCE, when the anomaly at Hawaii dropped 22 units below Easter Island. Hawaii then dropped to 29 units below Easter Island during CLIVAR.

So, did the $\Delta^{14}C$ at Hawaii go down, or did the $\Delta^{14}C$ at Easter Island go up? It would seem that Hawaii went down. During pre-bomb time, the $\Delta^{14}C$ at Hawaii was about 7-8‰ higher than the values at Palmyra and Fanning Islands north of the equator. During WOCE, the difference decreased to 5-6‰. But by the mid 2000s, the $\Delta^{14}C$ at Hawaii was indistinguishable from the $\Delta^{14}Cs$ in the equatorial band. The anomalies north of Hawaii also dropped from 0 and +1 during WOCE to −18 and −12 during CLIVAR. Meanwhile, Easter Island and the area north of New Zealand maintained their differences with the equatorial band. So, it would that the area between the equator and 30°N became lower in $\Delta^{14}C$ over time in relation to the South Pacific.

6. Anomaly Map for the Indian Ocean

Only two locations in the Indian Ocean have coral or shell measurements from 1940 to 1954. As such, the WOCE survey, carried out over fourteen months between December 1994 and January 1996, provides our only look at the Indian Ocean.

The Indian Ocean is a special place with respect to $\Delta^{14}C$. The WOCE measurements from the Indian Ocean are shown in **Figure 5** using the same color scale as the Pacific map in **Figure 2**. The contrast in color shades show that the surface waters of the Indian Ocean were 40-50‰ lower in $\Delta^{14}C$ on average than the surface waters in the Pacific. The anomaly map in **Figure 6** shows more clearly how these values were distributed. The reference value, in this case, is an arbitrary 90‰.

The largest anomaly in the Indian Ocean, −60, is from the northern Arabian Sea near the border between Yemen and Oman. The area off Oman is a well known upwelling area (Smith and Bottero, 1977). The −60 anomaly is derived from two locations. The location closer to the coast would have had an anomaly of −71 by itself (Region 3, **Table S6**). The next largest anomaly, −53, comes from four samples

collected along the west coast of India by Bhushan et al. (2000). This is also a coastal upwelling area (Luis and Kawamura, 2004).

Outside of the Arabian Sea, the next largest anomalies, −35 and −38, are from the area off central Sumatra. The −38 anomaly is from two locations near a coastal upwelling center at 4°S (Susanto et al., 2001). The −35 anomaly is from three locations that straddle the equator a few degrees to the north. Grumet et al. (2004) analyzed a coral collected at 0.1°S and found that the growth bands for the years 1944 to 1954 had an average $\Delta^{14}C$ of −65‰. This value is very similar to the pre-bomb $\Delta^{14}C$ in our Galapagos coral, −68‰. This finding is not surprising, perhaps, because the area off Sumatra is similar geographically to the area off Peru.

The Pacific Ocean is presumed to have had a relatively high in $\Delta^{14}C$ during WOCE because it has vast areas over which gas exchange can operate. The Indian Ocean, in contrast, has more areas of upwelling and a relatively small area for gas exchange. The upwelling areas therefore have more influence. This would explain why the Indian Ocean had such a low average $\Delta^{14}C$.

7. Surface $\Delta^{14}C$ Anomalies in an Ocean Circulation Model

CM2Mc is a low-resolution version of GFDL's coupled model CM2M (Dunne et al., 2012 and 2013) that was set up by Galbraith et al. (2011) to study the ocean's biogeochemical cycling. It is based on a 2.5° grid and has 28 levels in the vertical.

A finer resolution near the equator allows CM2Mc to have a stronger and better resolved Equatorial Undercurrent (EUC). CM2Mc also uses a low background vertical mixing coefficient of 0.1 $cm^2\ s^{-1}$ that minimizes the amount of abyssal water that is upwelled into the thermocline in low latitudes. CM2Mc includes separate tracers for $^{14}CO_2$ and $^{12}CO_2$ that are manipulated within its biogeochemistry module. ^{13}C is not simulated, so $\Delta^{14}C$ is simply $(^{14}CO_2/^{12}CO_2 - 1)\cdot 1000$.

Galbraith et al. (2011) describe the $\Delta^{14}C$ distribution in the model at the end of a long pre-industrial run. The surface distribution is shown in the **top panel of Figure 7**. Cross-basin $\Delta^{14}C$ differences in the model are only half as large as the pre-bomb differences documented here. Because the winds in the coupled model might be deficient, we

carried out a second pre-industrial run with an ocean-only version of CM2Mc that is forced with the observed winds.

The forcing in this case is from the normal year CORE-1 forcing described in Large and Yeager (2004) and Griffies et al. (2009). The surface distribution from this run is shown in the **bottom panel of Figure 7**. Cross-basin $\Delta^{14}C$ differences are a bit larger. The most notable change is in the northwest corner of the Pacific. The most notable difference in the wind forcing, however, is in the eastern equatorial Pacific where the winds in the coupled model basically fail to resolve the low-level convergence into the Intertropical Convergence Zone (ITCZ). This is important because the convergence into the ITCZ from the south drives the upwelling off Peru. The observed winds in the CORE-forced model manage to capture some of the upwelling.

Both model runs were extended to introduce the fossil-fuel and bomb perturbations. The $\Delta^{14}C$ values at Bermuda and Okinawa were then subtracted to create a set of anomaly maps like those in **Figures 3 and 4**. The anomalies for the Atlantic and Pacific from the CORE-forced model are shown in **Figures 8 and 9**, respectively. The observed anomalies have been overlaid as colored dots: when model and the observations are in agreement the colors in the background and the colors in the dots are the same.

7a. Data-Model Comparison in the Atlantic

The tropical Atlantic in the model is a very different place from the tropical Atlantic in the real ocean. The pre-bomb maps in **Figures 8a and 8b** show that the model expects anomalies of +4 off southern Brazil when the measured anomalies were −8. During the 1950s, the model expects an anomaly off northern Brazil of +1 when the measured anomaly was −16. The model expects an anomaly of +1 off Puerto Rico when the measured anomaly was −14. The WOCE map in **Figure 8c** shows that the model expects anomalies of +10 to +30 across the tropical Atlantic when the actual anomalies were between −22 and −37. These are very large differences.

The tropical Atlantic in the real ocean is low in $\Delta^{14}C$ because the northward flow of the AMOC is routed up to the surface off the coast of Africa. This is simply not happening in the model. The WOCE map in **Figure 8c** shows that the model manages to

bring a small amount of low-$\Delta^{14}C$ water up to the surface off southern Africa but the upwelled water does not spread much beyond the dateline.

The low-$\Delta^{14}C$ surface waters in the tropical Atlantic spread into the Caribbean Sea (Kilbourne et al., 2007) and are then carried northward off Florida (Schmitz and Richardson, 1991). As such, the surface waters off Florida have ^{14}C deficits of 10 to 16‰ relative to Bermuda. In contrast, the surface waters off Florida in our model are *higher* in $\Delta^{14}C$ than the surface waters off Bermuda. So, there is no low-$\Delta^{14}C$ water exiting from the tropics at the surface off Florida at all! All the negative anomalies in our model are north of Bermuda. This means that the northward flow of the AMOC in the model does not reach the surface until it crosses 30°N.

The scope of this failure is rather mind-boggling. It is easily understood, however, given the source of the problem. The upwelling in coastal upwelling zones generally takes place within 10-25 km of the coast (Huyer, 1983) whereas the grid cells in CM2Mc have dimensions of ~300 km. State-of-the-art climate models have resolutions of ~100 km. Models with these resolutions will not resolve this sort of upwelling.

7b. Data-Model Comparison in the Pacific

A departure of a different kind occurs in the Pacific. **Figure 9** shows the model's anomaly distributions during 1940-54, 1991-1993, and 2003-2006. Again, the observed anomalies are given by the colored dots. The largest discrepancies are found in the subpolar zone and along the coast of North America. The simulated anomalies off Kamchatka and in the Gulf of Alaska in our CORE-forced model are some 40 units smaller than observed (**Figure 9b**). Too much high-$\Delta^{14}C$ water from the subtropics is being carried northward into the subpolar gyre. The anomalies off Kamchatka in our coupled model (not shown) are 100 units smaller than observed!

Maps of the steric height relative to 1500 m (not shown) indicate that the upper ocean in our coupled model is too thick. The extra thickness is due to a greater vertical spread between the 6, 8, and 10° isotherms. These are the isotherms that bracket SAMW in the South Pacific (McCartney, 1977). The thickness of these layers drives a shallow

overturning circulation that is responsible for these discrepancies. Overturning stream functions for the IndoPacific region are shown in **Figure 10**.

The overturning from the coupled model in the **top panel of Figure 10** includes a shallow cell in the North Pacific in which more than 4 Sv of water flows northward near the surface and sinks north of 50°N. The sinking water then flows back to the south above 1200 m and connects up with the upwelling along the equator. The same cell is present in the CORE-forced model in the **bottom panel of Figure 10** but is not as strong. As shown in the maps in **Figure 9**, even the relatively weak cell in the CORE-forced model has a deleterious effect on the surface $\Delta^{14}C$.

The subsurface component of the shallow overturning cell picks up low-$\Delta^{14}C$ water from the deep ocean and carries it across 10°N into the equatorial zone. The low-$\Delta^{14}C$ water is then delivered up to the surface as the flow into the equatorial zone veers back to the east along with the EUC. The re-emergence of the subpolar water can be seen in the contrast between the two models in **Figure 7** where the surface $\Delta^{14}C$ values are distinctly lower north of the equator in the coupled model. The net result is that the subpolar zone in the coupled model is much too high in $\Delta^{14}C$ while the area between the equator and 10°N is too low in $\Delta^{14}C$.

We see the shallow overturning cell as a buoyancy-forced circulation that develops in our model because of the lack of upwelling off Peru. North-south temperature sections through the Pacific show that the 5° isotherm reaches 1000 m at 50°S. SAMW accounts for most of the water above the 5° isotherm (http://www-pord.ucsd.edu/whp_atlas/pacific/p16/sections/printatlas/printatlas.htm). The isopycnals within the SAMW layers then shoal north of 30°N in the North Pacific. There is more shoaling in our model because the SAMW isopycnals start off at greater depths in the South Pacific.

We see the buoyancy contrast denoted by the shoaling isopycnals as the energy source for the shallow overturning cell. The shallow overturning cell is too strong in our model because the north-south buoyancy contrast is overly large. The upwelling off Peru is relevant because it extracts mass from the SAMW layers. There is no extraction in our coupled model because the winds in the model do not resolve the upwelling off Peru.

Without this extraction, the SAMW layers remain overly thick and the buoyancy contrast in the North Pacific remains overly large.

This is not to say that the shallow overturning in the model does not exist. Low-salinity, high-silica water is known to flow into the equatorial zone from the North Pacific (Dugdale et al., 2002). This water seems to have a clear affinity with the low-salinity, high-silica subpolar water in the California Current (see below). Low-$\Delta^{14}C$ subpolar water is also seen to penetrate into the eastern equatorial Pacific during the positive phase of the Pacific Decadal Oscillation (Druffel et al., 2014).

8. Discussion

The upwelling around the ocean's margins and the upwelling associated with the ocean's overturning have always been seen as separate entities. This is largely because the upwelling around the margins is thought to have a limited vertical extent. There is a solid basis for this expectation: the water upwelling around the margins seems to be too warm to have an origin in the deep ocean.

TDB91 showed, however, that the water upwelling off Peru is lower in $\Delta^{14}C$ than one would expect from its temperature. The reason is that the mode water-bearing layers of the South Pacific – the source of the water upwelled off Peru – are warmed by mixing with the warmer water above while the $\Delta^{14}C$ of the layers is barely altered. TDB91 estimated that the mode water-bearing layers are warmed in this way by about 6°C. Thus, upwelled water that may appear to be thermocline water is actually from greater depths. The key to this distinction is the weak coupling of $\Delta^{14}C$ to the atmosphere. For a more complete discussion, the reader is referred to the discussion in TDB91 that accompanies their Figure 16. The results above show that the kind of upwelling seen off Peru seems to occur along the eastern boundaries of all three ocean basins.

The Discussion below considers the larger significance of the eastern boundary upwelling. Our claim is that the eastern boundary upwelling is no less important for the ocean's overturning than the upwelling in the Southern Ocean. This claim is developed in three sections. The first, 8a, shows that there is a clear distinction between the eastern boundary upwelling and the upwelling in the subpolar zone of the North Pacific. The

second, 8b, makes use of a simple two-dimensional diagram to illustrate how the eastern boundary upwelling contributes to the overturning. The third, 8c, shows how the upwelling off Africa contributes to the northward heat transport of the AMOC.

8a. $\Delta^{14}C$ and Thermocline Nutrients

Sarmiento et al. (2004) showed that the main way for nutrients to be cycled from the deep ocean back up to the upper ocean is via the upwelling south of the ACC. Their demonstration was based on the relative concentrations of silica and nitrate.

Deep water generally has more silica than nitrate but much of the silica is removed from the deep water that upwells south of the ACC. (The microplankton of the Southern Ocean are known to take up silica preferentially over nitrate, Brzezinski et al., 2003). As a result, the SAMW that is formed north of the ACC has less silica than nitrate. Sarmiento et al. showed that lower thermocline waters across most of the ocean are silica-poor in the same way, and they attributed the dearth of silica to the SAMW just below. On the other hand, the lower thermocline waters of the North Pacific were found to have more silica than nitrate. Sarmiento et al. traced this composition to silica-rich deep water that manages to poke through into the upper ocean in the northwest corner of the Pacific basin.

A similar pattern is seen here in the water that is upwelled around the margins. To illustrate this effect we have plotted the $\Delta^{14}C$ values used to construct our Pacific averages for the WOCE Era in **Table S4** against the salinities measured in the same samples. The left hand panel of **Figure 11** shows the results from the North Pacific. Points from the same regions are enclosed and labeled accordingly. $\Delta^{14}C$ co-varies with salinity in the North Pacific in a simple way. Two compositions dominate. One is salty and high in $\Delta^{14}C$ and comes from the area north of Hawaii along 30°N (Regions 8 and 9). This end member is influenced by the evaporation in the subtropics and the exchange of CO_2 with the atmosphere. The other end member is relatively fresh and low in $\Delta^{14}C$ and comes from the area off Kamchatka (Region 2).

A mixing line between the two end-members has been drawn by eye on the plot. The surface waters off Southern California (Region 7), Baja California (Region 11), and

Guatemala (Region 13) appear to be simple mixtures of the two end members. Basically, the North Pacific Drift flows eastward across the Pacific between the areas where the two end members are formed. The Drift then splits into the California Current and the Alaska Current as it approaches North America. The upwelling zones off North America and Central America seem to tap into different mixtures of the subtropical and subpolar water types in the California Current.

The Alaska Current, meanwhile, receives a heavy input of fresh water from the runoff along the coast. The runoff makes the points from Sitka, Alaska (Region 4) and the points from the Gulf of Alaska (Region 3) diverge from the mixing line. But as with the upwelling off Southern California, the upwelling off Alaska does not tap into the deep ocean directly. Rather it seems to draw up water that was originally drawn up from the deep ocean near Kamchatka.

The right-hand panel of **Figure 11** is an equivalent plot for the South Pacific. The North Pacific mixing line is shown for reference. Fifteen points, plotted with open circles, have been added to complete the picture; these are not from any of the regions in **Table S4**. The five open circles labeled "subantarctic zone" are from the northern edge of the ACC. The four open circles at the bottom are from the polar front further south. Six open circles with moderately high $\Delta^{14}C$ values represent the relatively fresh surface waters off southern Chile (35 to 50°S).

Distinctly different end-members characterize the water that reaches the surface in the eastern equatorial Pacific. The eastern Pacific end-members are highlighted by the blue dots in **Figure 11**. These compositions are moderately low in $\Delta^{14}C$ and differ mainly in their salinity. The salty end member is from Peru (Region 30 in **Figure 11b**). The fresh end member comes from the area under the ITCZ north of the equator (Region 17 in **Figure 11a**). A second mixing line connects these compositions (nearly horizontal red lines). Points from the Galapagos Islands (Region 24) appear on both of the plots and fall along the red line that is drawn through the points from Peru and the ITCZ.

The lowest $\Delta^{14}C$ values in the ITCZ region come from an upwelling feature known as the Costa Rica Dome. Kessler (2006) shows that the water upwelling in the Dome has the same subantarctic source as the water upwelling off Peru. The upwelled

water becomes fresh after it is brought up to the surface in the ITCZ. Like the upwelling off Peru, the upwelling in the Costa Rica Dome is driven by winds that converge into the ITCZ. The convergence in this case comes from the east through gaps in the mountains of Central America.

In summary, the results here are consistent with Sarmiento et al. (2004) in showing that deep water is brought into the upper Pacific two ways. In one, deep water is upwelled initially in the Southern Ocean and is injected below the thermocline north of the ACC. This water has less silica than nitrate and is drawn up to the surface a second time in the eastern boundary upwelling zones off Costa Rica and Peru. In the other, deep water that is high in silica and low in $\Delta^{14}C$ is drawn directly up to the surface in the northwest off Kamchatka.

8b. Thin Upper Ocean

The upwelling zones off Costa Rica, Peru and Kamchatka are able to tap into the deep water below the thermocline because the upper ocean is thin in these areas. The easterly winds in the tropics tilt the thermocline up in the east so that the subantarctic water below the thermocline is only 100 m or so below the surface off Costa Rica and Peru. Similarly, the geostrophic flow in the subpolar gyre (the flow that balances the equatorward flow out of the gyre in the surface Ekman layer) makes the isopycnals in the subpolar gyre tilt up toward the west. These tilts put the deep water below within range of the Ekman pumping at the surface.

In this context, the upper ocean is often described as a "bowl" of low-density fluid that floats in a large volume of denser fluid (e.g. Toggweiler and Samuels, 1998; Gnanadesikan, 1999). The upwelling off Oman and Kamchatka is clearly able to tap into the deep water below the bowl. It would seem in this regard that the bowl of low-density fluid is sufficiently thin *in general* that the Ekman pumping can reach the bottom of the bowl in places where the tilts permit. The Ekman pumping in our model, meanwhile, has a hard time reaching the bottom of the bowl anywhere.

The bowls in ocean models are famous for being overly thick. This is usually attributed to thermoclines that are too diffuse (Randall et al., 2007) but the largest errors

in model temperature fields are actually below the thermocline. Figure 8.9 from Randall et al. (2007) is reproduced here as **Figure 12**. The temperature error from a multi-model mean (color shading) is overlaid on a north-south section of the observed zonally averaged temperature. The overlay shows that model temperatures are especially warm between the 5 and 10° isotherms. This is the domain of the mode and intermediate waters that are formed north of the ACC, the lower part of the bowl.

The thickness of the upper ocean was once thought to reflect a balance between vertical mixing and the upwelling of deep water from below. Gnanadesikan (1999) reframed the problem by showing how the bowl is filled in the south. His approach is illustrated in the **top panel of Figure 13**. Deep water is drawn up to the surface by the winds that drive the ACC. The deep water is then added to the bowl as it is warmed and freshened from the atmosphere. Water is removed from the bowl when it is transformed into North Atlantic Deep Water (NADW) in the North Atlantic. Processes that diminish the inflow in the south or enhance the outflow in the north make the bowl thinner.

The approach behind the top panel was seen as a breakthrough in its day because it showed how the ocean's overturning can operate with very little vertical mixing. We would argue here that it only gets half way to the low-mixing limit. It is missing a critical element, as is illustrated in the **bottom panel of Figure 13**. In this case, the water added to the bowl in the Southern Ocean is identified as SAMW/AAIW and is added to the lower part of the bowl between the 5 and 10° isotherms. NADW, meanwhile, is shown being drawn from the upper part of the bowl. (The justification for this assertion is given in the next section.) This leaves a gap that is bridged when SAMW/AAIW is upwelled from the lower part of the bowl into the upper part off Africa.

The precursors of NADW are very different in the two views. Once drawn to the surface, the precursors in the bottom panel are exposed to the salinification that is known to take place in the tropical and subtropical Atlantic. They are exposed to the cooling in the North Atlantic. Hence, NADW is formed and removed from the bowl more readily for a given input in the south. This is arguably what makes the upper ocean thin. A similar argument can be made for the Pacific where the upwelling off Costa Rica and Peru transforms SAMW into a lighter water type that is able to leave the Pacific via the

Indonesian Seas (Kessler, 2006; McCreary et al., 2007). This leads us to conclude that the upwelling off Oman and Kamchatka is able to tap into deep water because the eastern boundary upwelling makes the upper ocean generally thin.

The overturning in ocean models is more like the situation in the **top panel of Figure 13**. The eastern boundary upwelling is missing or too weak and SAMW/AAIW is not brought up to the surface from the lower part of the bowl. As a result, the inflow from the ACC tends to remain in the lower part of the bowl where the extra thickness in ocean models does, in fact, reside (**Figure 12**). The extra thickness in our coupled model gives rise to the shallow overturning in the **top panel of Figure 10** that carries an excessive amount of subtropical water into the subpolar gyre.

8c. Impact on Heat Transport

The Florida Current carries about 32 Sv of water across 26.5°N through a narrow passage that is about 800 m deep (Schmitz and Richardson, 1968; Johns et al., 2011). According to Schmitz and Richardson (1991), the AMOC accounts for about 45% of the overall flow. As alluded to earlier, the AMOC portion is separated vertically: 60% of the northward flow is at or near the surface with temperatures >24°C; the remaining 40% flows northward just above the bottom with temperatures between 7 and 12°C (Schmitz and Richardson, 1991). It goes without saying that the AMOC's northward heat transport is carried mainly by the surface component. Using a high-resolution ocean model, Xu et al. (2012) determined more recently that the AMOC's flow across 26.5°N consists of "2/3 surface water and 1/3 AAIW."

Schmitz and Richardson (1991) did not venture to say why the AMOC is divided this way but Schmitz and McCartney (1993) took up the challenge. They recognized that the surface and intermediate components off Florida are both derived from a cool subantarctic source that enters the South Atlantic across 32°S. In this context, the 7-12° component was seen as a slightly warmed version of the inflow. They then suggested, somewhat sheepishly, that the >24° component is "upwelled into the surface layer as a result of the Ekman divergence near the equator." The warming implications of this suggestion are hard to swallow. The coolest sea surface temperatures (SSTs) near the equator are about 22° (Mitchell and Wallace, 1992). If the >24° component were to be brought to the

surface near the equator, most of the warming would have to take place before the water reaches the surface. A huge amount of mixing would be required to warm the inflow by this amount.

The results here would suggest that the inflow is brought to the surface off Africa where the SSTs are cooler. The coolest SSTs off Namibia, for example, are about 16° (Lutjeharms and Meeuwis, 1987). Gordon et al. (1995) show that the upwelling off Namibia is fed from a shallow subsurface flow on the Namibian shelf with a temperature of about 12°C. If the >24° component were to be brought to the surface off Namibia, the warming of the inflow from 12 to 24° would all take place at the surface in response to the upwelling. Much less mixing would be needed.

The upwelling off Africa is driven by winds along the African coast that are quite independent of the overturning. Thus, the upwelling can occur or not occur. It follows that the AMOC would remain confined to the 7-12° layer if the upwelling off Africa did not occur. The heat transport off Florida would then be greatly reduced. On the other hand, more of the northward flow is brought up to the surface if the upwelling is strong. More heat is taken up from the atmosphere and the heat transport is greatly enhanced. The implications are quite profound: most of the heat that is taken up and exported from the tropical Atlantic via the AMOC may be a direct response to the winds off Africa.

Ocean models are famous for having a northward heat transport in the Atlantic that is systematically too weak (see Griffies et al. 2014). Our sense is that the cause is a weak surface flow in the Florida Current that is due to the missing upwelling off Africa (**Figures 8c and 8d**). We would note in this regard that the strong surface flow across 26.5°N in Xu et al. (2012) is from a model that is limited to the Atlantic basin north of 28°S. A sponge layer between 25° and 28°S converts the outflow of NADW into an inflow above. The upwelling zone off Namibia happens to lie within the sponge layer. So, the surface flow coming out of the upwelling zone in the real ocean should be part of the flow coming out of the sponge layer whether the upwelling itself is resolved by the model or not.

10. Conclusions

^{14}C deficits are generated in the deep ocean and erased at the surface. Large deficits at the surface are an indication that water from the deep ocean has been raised to the surface. Here we find a fairly simple pattern in the distribution of ^{14}C deficits north of the ACC. The largest deficits are found in the upwelling zones off Oman and Kamchatka in the northwest corners of the Indian and Pacific Oceans. The deficits in these areas come from deep water that is drawn directly up to the surface. The largest ^{14}C deficits in the tropics are found in the eastern boundary upwelling zones off Africa, off Costa Rica and Peru, and off Sumatra in the Indian Ocean. The deficits in these areas can be traced back to the mode and intermediate waters that are formed along the northern edge of the ACC.

The mode and intermediate waters from the ACC are the water masses that are converted into NADW in the North Atlantic. It would appear that 60% or more of the water that becomes NADW is raised to the surface in the upwelling zones off the coast of Africa. As such, the upwelling off Africa is an important part of the AMOC and a major contributor to the ocean's heat transport and vertical structure. The upwelling helps explain, in particular, how a large northward heat transport can exist in the Atlantic with relatively little vertical mixing. The upwelling off Africa is therefore no less important to the ocean's overturning and heat transport than the upwelling along the ACC.

Acknowledgements

This study is based on hundreds of $\Delta^{14}C$ measurements made by other investigators. We would first like to acknowledge the important contributions made by all the people who produced the measurements that are compiled in the Supplemental Material; we apologize for the fact that these contributions are not cited in the text. Funding for the WOCE and CLIVAR measurements was provided by NSF and NOAA. The measurements were carried out at the National Ocean Sciences Accelerator Mass Spectrometry Facility (NOSAMS) at the Woods Hole Oceanographic Institution under the supervision of Ann McNichol and Karl von Reden. ERMD would like to acknowledge support from the NSF Chemical Oceanography program (OCE-0551940 and OCE0961980). RMK received support from NSF ^{14}C CLIVAR grant OCE-0825163 and its predecessors. Model simulations were carried out on the Scinet cluster using a resource allocation to EDG from Compute Canada. John Dunne, Matt Harrison, Bob Hallberg, and Steve Griffies made valuable suggestions that have improved the paper. Jeff Varanyak and Brendan Carter provided help with the figures; Gail Haller helped with the references.

References

Bhushan, R., B. L. K. Somayajulu, S. Chakraborty, and S. Krishnaswami, Radiocarbon in the Arabian Sea water column: Temporal variations in bomb ^{14}C inventory since GEO-SECS and CO_2 air-sea exchange rates, J. Geophys. Res., 105(C6), 14273-14282, 2000.

Broecker, W. S., and T.-H. Peng, Gas exchange rates between air and sea, Tellus, 26, 21-35, 1974.

Broecker, W. S., T.-H. Peng, H. G. Ostlund, and M. Stuiver, The distribution of bomb radiocarbon in the ocean, J. Geophys. Res., 90, 6953-6970, 1985.

Brzezinski, M. A., M-L dickson, D. M. Nelson, and R. Sambrotto, Ratios of Si, C, and N uptake by microplankton in the Southern Ocean, Deep-Sea Res. II, 50, 619-633, 2003.

Dewar, G., P. J. Reimer, J. Sealy, and S. Woodborne, Late-Holocene marine radiocarbon reservoir correction (ΔR) for the west coast of South Africa, The Holocene, 22(12), 1481-1489, 2012.

Drijfhout, S. S., D. P. Marshall, and H. A. Dijkstra, Conceptual models of the wind-driven and thermohaline circulation, in *Ocean Circulation and Climate: A 21st Century Perspective*, edited by G. Siedler, S. M. Griffies, J. Gould, and J. A. Church, Elsevier, Amsterdam, 257-282, 2013.

Druffel, E. R. M., Radiocarbon in annual coral rings from the eastern tropical Pacific Ocean, Geophys. Res. Lett., 8, 59-62, 1981.

Druffel, E. R. M., Decade time scale variability of ventilation in the North Atlantic: High precision measurements of bomb radiocarbon in banded corals, J. Geophys. Res., 94(C3), 3271-3285, 1989.

Druffel, E. M. and T. W. Linick, Radiocarbon in annual coral rings of Florida, Geophys. Res. Lett., 5, 913-916, 1978.

Druffel, E. R. M., J. E. Bauer, and S. Griffin, Input of particulate organic and dissolved organic carbon from the Amazon to the Atlantic Ocean, Geochem. Geophys. Geosyst., 6(3), doi:1029/2004GC000842, 2005.

Druffel, E. R. M., S. Beaupre, S. Griffin, and J. Hwang, Varibiability of dissolved inorganic radiocarbon at a surface site in the Northeast Pacific Ocean, Radiocarbon, 52, 1150-1157, 2010.

Druffel, E. R. M., S. Griffin, D. S. Glynn, R. B. Dunbar, D. A. Mucciarone, and J. R. Toggweiler, Seasonal radiocarbon and oxygen isotopes in a Galapagos coral: Calibration with climate indices, Geophys. Res. Lett., 41, 5099–5105, doi:10.1002/2014GL060504, 2014.

Dugdale, R. C., A. G. Wischmeyer, F. P. Wilerson, R. T. Barber, F. Chai, M.-S Jiang, and T.-H. Peng, Meridional asymmetry of source nutrients to the equatorial Pacific upwelling ecosystem and its potential impact on ocean-atmosphere CO2 flux; a data and modeling approach, Deep-Sea Res. II, 49, 2513-2531, 2002.

Dunne, J. P. et al., GFDL's ESM2 global coupled climate-carbon Earth System Models Part I: Physical formulation and baseline simulation characteristics, J. Climate, 25, 6646-6665, 2012.

Dunne, J. P. et al., GFDL's ESM2 global coupled climate-carbon Earth System Models Part II: Carbon system formulation and baseline simulation characteristics, J. Climate, 26, 2247-2267, 2013.

Eiríksson, J. et al., Coupling of paleoceaographic shifts and changes in marine reservoir ages off North Icealnd through the last millennium, Palaeogeogr., Palaeoclim., Palaeoecol., 302, 95-108, 2011.

Fallon, S. J. and T. P. Guilderson, Surface water processes in the Indonesian throughflow as documented by a high-resolution coral $\Delta^{14}C$ record, J. Geophys. Res., 113, C09001, doi:10.1029/2008JC004722, 2008.

Galbraith, E. D. et al., Climate variability and radiocarbon in the CM2Mc Earth System Model, J. Climate, 24, 4230-4254, doi:10.1175/2011JCLI3919.1, 2011.

Gnanadesikan, A., A simple predictive model for the structure of the oceanic pycnocline, Science, 283, 2077-2079, 1999.

Goodkin, N. F., E. R. M. Druffel, K. A. Hughen, and S. C. Doney, Two centuries of limited variability in subtropical North Atlantic thermocline ventilation, Nature Commun., 3:803, doi: 10.1038/ncomms1811, 2012.

Gordon, A. L., R. F. Weiss, W. M. Smethie, and M. J. Warner, Thermocline and intermediate water communication between the South Atlantic and Indian Oceans, J. Geophys. Res., 97(C5), 7223-7240, 1992.

Gordon, A. L., K. T. Bosley, and F. Aikman, Tropical Atlantic Water within the Benguela Upwelling system at 27°S, Deep-Sea Res. I, 42(1), 1-12, 1995.

Griffies, S. M. et al., Coordinated ocean-ice reference experiments (COREs), Ocean Modelling, 26(1-2), 1-46, doi:10.1016/j.ocemod.2008.08.007, 2009.

Griffies, S., M. et al., Impacts on ocean heat from transient mesoscale eddies in a hierarchy of climate models, J. Climate, doi:10.1175/JCLI-D-14-00353.1, in press.

Grumet, N. S. et al., Coral radiocarbon records of Indian Ocean water mass mixing and wind-induced upwelling along the coast of Sumatra, Indonesia, J. Geophys. Res., 109, C05003, doi:10.1029/2003JC002087, 2004.

Huyer, A., Coastal upwelling in the California Current system, Prog. Oceanogr., 12, 259-284, 1983.

Johns W. E. et al., Continuous, array-based estimates of the Atlantic Ocean heat transport at 26.5N, J. Climate, 24, 2429-2449, 2011.

Jónsson, S. and H. Valdimarsson, Water mass transport variability to the North Icelandic shelf, 1994-2010, ICES J. Marine Science, doi:10.1093/icejms/fss024, 2012.

Kessler, W. S., The circulation of the eastern tropical Pacific: a review, Prog. Oceanogr., 69, 181-217, 2006.

Kilbourne, K. H., T. M. Quinn, T. P. Guilderson, R. S. Webb, and F. W. Taylor, Decadal- to interannual-scale source water variations in the Caribbean Sea recorded by Puerto Rican coral radiocarbon, Clim. Dyn., 29, 51-62, 2007.

Knudsen, K. L., J. Eiríksson, E. Jansen, J. Jiang, F. Rytter, and E. R. Gudmundsdóttir, Palaeoceanographic changes off North Iceland through the last 1200 years, Quat. Sci. Rev., 23, 2231-2246, 2004.

Konishi, K. T. Tanaka, and M. Sakanoue, Secular variation of radiocarbon concentration in seawater: sclerochronological approach, In *Proceedings of the Fourth International Coral Reef Symposium, vol. 1*, edited by E. D. Gomez, pp. 181-185, Marine Science Center, University of the Philippines, Manila, 1982.

Large W. and S. Yeager, Diurnal to decadal global forcing for ocean and seaice models: the data sets and climatologies, Technical Report TN-460+STR, NCAR, 105 pp, 2004.

Luis, A. J. and H. Kawamura, Air-sea interaction, coastal circulation, and primary production in the eastern Arabian Sea: a review, J. Oceanography, 60, 205-218, 2004.

Lutjeharms, J. R. E. and J. M. Meeuwis, The extent and variability of South-east Atlantic upwelling, In *The Benguela and Comparable Ecosystems*, South African Journal of Marine Science, 5, 51-62, 1987.

Marshall, J. and K. Speer, Closure of the meridioanl overutnring circulation through Southern Ocean upwelling, Nature Geoscience, 5, 171-180, 2012.

Massé, G., S. J. Rowland, M-A Sicre, J. Jacob, E. Jansen, and S. T. Belt, Abrupt climate changes for Iceland during the last millennium: Evidence from high-resoltuion sea-ice reconstructions, Earth Planet. Sci. Lett., 269, 565-569, 2008.

McCartney, M. S., Subantarctic mode water, in *A Voyage of Discovery*, edited by M. Angel, Pergamon, Oxford, 103-119, 1977.

McCreary, J. P., T. Miyama, R. Furue, T. Jensen, H.-W. Kang, B. Bang, and T. Qu, Interactions between the Indonesian Throughflow and circulations in the Indian and Pacific Oceans, Prog. Oceanogr., 75, 70-114, 2007.

McDuffee, K. and E. R. M. Druffel, Daily variability of dissolved inorganic radiocarbon in Sargasso Sea surface water, Mar. Chem., 106, 510-515, 2007.

Mitchell, T. P. and J. M. Wallace, The annual cycle in equatorial convection and sea surface temperature, J. Climate, 5, 1140-1156, 1992.

Mittelstaedt, E., The upwelling area off northwest Africa – a description of phenomena related to coastal upwelling, Prog. Oceanogr., 12, 307-331, 1983.

Nelson, G. and L. Hutchings, The Benguela upwelling area, Prog. Oceanogr., 12, 333-356, 1983.

Nydal, R., Carbon-14 measurements in surface water CO_2 from the Atlantic, Indian, and Pacific Oceans, 1965-1994, A. Brenkert and T. Boden, editors, ORNL/CDIAC-104, NDP-057A, Carbon Dioxide Information Analysis Center, Oak Ridge National Laboratory, Oak Ridge, TN, pp. 131, 1998.

Randall, D.A. et al., Climate Models and Their Evaluation (Chapter 8), in *Climate Change 2007: The Physical Science Basis*. *Contribution of Working Group I to the Fourth Assessment Report of the Intergovernmental Panel on Climate Change*, edited by S. Solomon et al., Cambridge University Press, Cambridge, UK, 996 p., 2007.

Sarmiento, J. L., N. Gruber, M. A. Brzezinski, J. P. Dunne, High-latitude controls of thermocline nutrients and low latitude biological productivity, Nature, 427, 56-60, 2004.

Schmitz, W. J. and M. S. McCartney, On the North Atlantic Circulation, Rev. Geophys., 31, 29-49, 1993.

Schmitz, W. J. and P. L. Richardson, On the transport of the Florida Current, Deep-Sea Res., 15, 679-693, 1968.

Schmitz, W. J. and P. L. Richardson, On the sources of the Florida Current, Deep-Sea Res., 38, Suppl. 1., S379-S409, 1991.

Sloyan, B. M. and S. R. Rintoul, Circulation, renewal, and modification of Antartctic mode and intermediate water, J. Phys. Oceanogr., 31, 1005-1030, 2001.

Smith, R. L. and J. S. Bottero, On upwelling in the Arabian Sea, in *A Voyage of Discovery*, edited by M. Angel, Pergamon Press, Oxford, 291-304, 1977.

Stuiver, M. and H. A. Polach, Reporting of ^{14}C data, Radiocarbon, 19, 355-363, 1977.

Stuiver, M., P. D. Quay, and H. G. Ostlund, Abyssal water carbon-14 distribution and the age of the World Oceans, Science, 219-849-851, 1983.

Susanto, R. D., A. L. Gordon, and Q. Zheng, Upwelling along the coasts of Java and Sumatra and its relation to ENSO, Geophys. Res. Lett., 28, 1599-1602, 2001.

Tanaka, N., M. C. Monaghan, and K. K. Turekian, ^{14}C balance for the Gulf of Maine, Long Island Sound, and the northern Middle Atlantic Bight: Evidence for the extent of Antarctic Intermediate Water contribution, J. Marine Res., 48, 75-87, 1990.

Toggweiler, J. R., K. Dixon, and W. Broecker, The Peru Upwelling and the ventilation of the South Pacific thermocline, J. Geophys. Res., 96(C11), 20467-20497, 1991.

Toggweiler, J. R. and B. Samuels, New radiocarbon constraints on the upwelling of abyssal water to the ocean's surface, in *The Global Carbon Cycle*, edited by M. Heimann, NATO ASI Series, Vol. I 15, Springer-Verlag, Berlin, 333-366, 1993.

Toggweiler, J. R. and B. Samuels, On the ocean's large-scale circulation near the limit of no vertical mixing, J. Phys. Oceanogr., 28, 1832-1852, 1998.

Xu, X., W. J. Schmitz, H. E. Hurlburt, and P. J. Hogan, Mean Atlantic meridional overturning circulation across 26.5°N from eddy-resolving simulations compared to observations, J. Geophys. Res., 117, C03042, doi:10.1029/2001JC007586, 2012.

Figure Captions

Figure 1. Time series of $\Delta^{14}C$ in three Atlantic corals, Florida Keys (Druffel and Linick, 1978; Druffel unpublished), Puerto Rico (Kilbourne et al., 2007), and the south coast of Bermuda (Druffel, 1989; Goodkin et al. 2012).

Figure 2. Surface distribution of $\Delta^{14}C$ in the Pacific Ocean based on seawater samples collected between 1991 and 1996 during WOCE.

Figure 3. Surface $\Delta^{14}C$ anomalies in the Atlantic during pre-bomb time **a)** during the 1940s, Bermuda $\Delta^{14}C = -47‰$, and **b)** during 1950-1954, Bermuda $\Delta^{14}C = -48‰$. **c)** during the main interval of WOCE sampling (1990-94), Bermuda $\Delta^{14}C = 113‰$, **d)** during 1997-98, Bermuda $\Delta^{14}C = 94‰$, and **e)** during CLIVAR (2003-05), Bermuda $\Delta^{14}C = 81‰$.

Figure 4. Surface $\Delta^{14}C$ anomalies in the Pacific **a)** during pre-bomb time 1940-1954, Okinawa $\Delta^{14}C = -40‰$, and **b)** during WOCE (1991-93), Okinawa $\Delta^{14}C = 115‰$, and **c)** during CLIVAR (2003-06), Okinawa $\Delta^{14}C = 90‰$.

Figure 5. Surface distribution of $\Delta^{14}C$ in the Indian Ocean based on seawater samples collected between December 1994 and January 1996 during WOCE.

Figure 6. Surface $\Delta^{14}C$ anomalies in the Indian Ocean relative to an arbitrary reference value of 90‰.

Figure 7. Surface $\Delta^{14}C$ from the fully coupled version **(top)** and the CORE-forced version **(bottom)** of CM2Mc at the end of pre-industrial time.

Figure 8. Anomaly pattern for the Atlantic from the CORE-forced version of CM2Mc with measured anomalies overlaid as colored dots **a)** during the 1940s, **b)** during 1950-54, **c)** during WOCE (1990-94), and **d)** during CLIVAR (2003-2005).

Figure 9. Anomaly pattern for the Pacific from the CORE-forced version of CM2Mc compared with the measured anomalies overlaid as colored dots **a)** during 1940-54, **b)** during WOCE (1991-93), and **c)** during CLIVAR (2003-2006).

Figure 10. Meridional overturning stream functions for the IndoPacific region from the coupled version of CM2Mc (**top**) and the CORE-forced version (**bottom**).

Figure 11. $\Delta^{14}C$ vs. salinity relationships for the eastern North Pacific **(a)** and South Pacific **(b)** based on the WOCE observations in **Table S4**. Open circles in **(b)** are from stations 48, 49, 51, and 56 on Line P15S ("polar front zone"), 65 on P15S, 35 on P16A, 37 on P18, and 258 and 261 on P19C ("subantarctic zone"), and 267, 274, 278, 287, 291, and 295 on Line P19C. Points from the N. Pacific and eastern equatorial zone follow nearly orthogonal trajectories (red lines). Blue points denote the extrema of the eastern equatorial trajectory. The blue points in **(a)** are from the ITCZ (Region 17); the blue points in **(b)** are from the area off Peru (Region 30).

Figure 12. Time-mean potential temperature zonally averaged over all ocean basins (black contours) and average model temperature error (color shading) from Chapter 8 of the IPCC Fourth Assessment Report. Observed temperatures are from the World Ocean Atlas 2004. Copied from Figure 8.9 in Randall et al. (2007).

Figure 13. (a) Illustration showing how the bowl of low-density fluid in the upper ocean is filled in the south, via the upwelling along the ACC, and drained in the north, via the formation of NADW. Adaped from Gnanadesikan (1999). The bottom of the bowl is the 5° isotherm. **(b)** Modification in which the bowl is divided into upper and lower layers. The internal boundary is the 10° isotherm. SAMW/AAIW is added to the lower layer. NADW is removed from the upper layer. Upwelling in the eastern boundary upwelling zones shifts SAMW/AAIW from the lower layer into the upper layer.

925

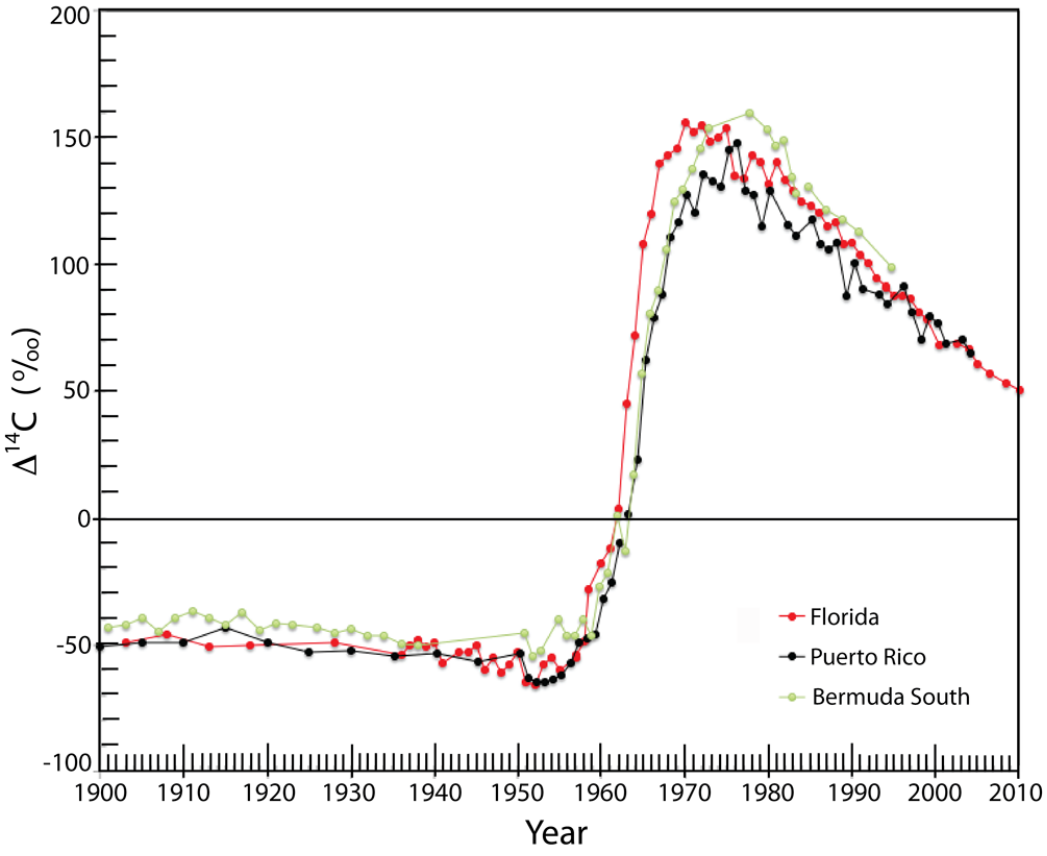

930

Figure 1. Time series of $\Delta^{14}C$ in three Atlantic corals, Florida Keys (Druffel and Linick, 1978; Druffel unpublished), Puerto Rico (Kilbourne et al., 2007), and the south coast of Bermuda (Druffel, 1989; Goodkin et al. 2012).

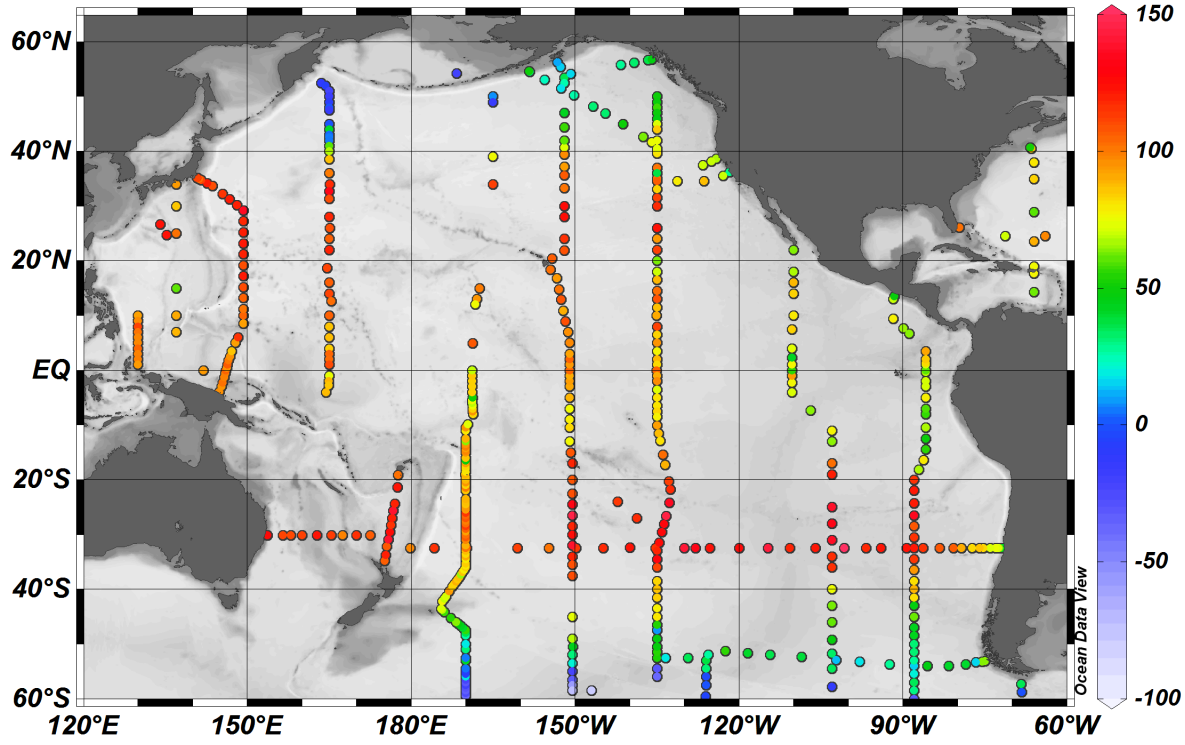

935

Figure 2. Surface distribution of $\Delta^{14}C$ in the Pacific Ocean based on seawater samples collected between 1991 and 1996 during WOCE.